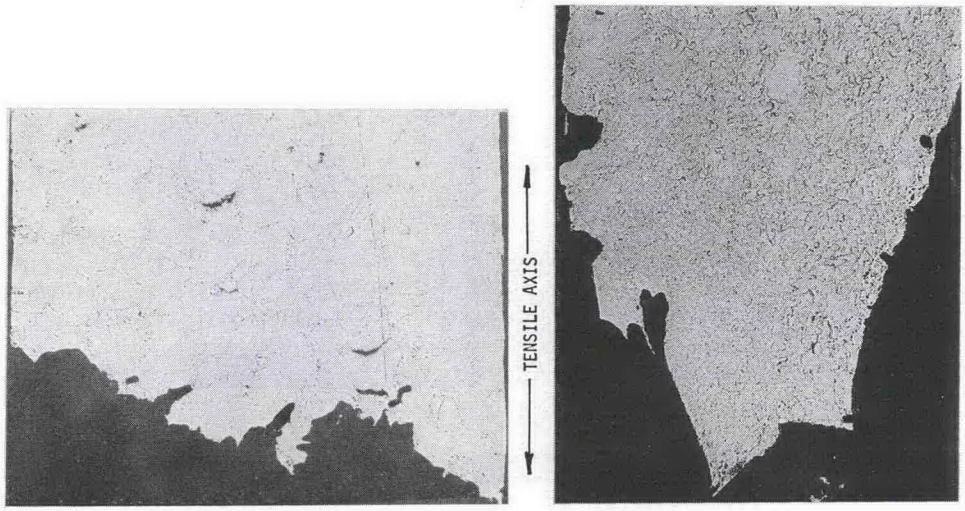

FIG. 10. The microstructure of 90% Sn–bal Bi specimens immediately behind the fracture surface in specimens tested to failure at: (a) atmospheric pressure, and (b) 1.5×10^8 N/m^2. 50×, Etched.

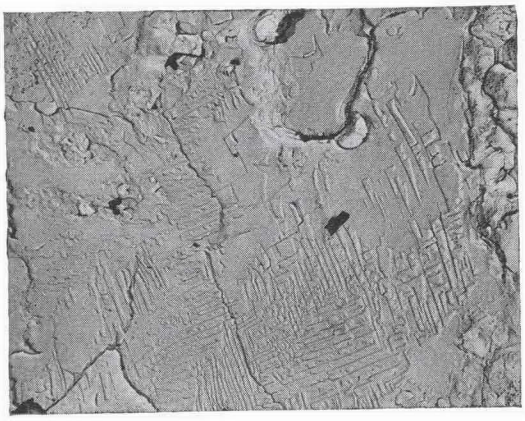

FIG. 11(a). An electron fractograph of a 90% Sn–bal Bi specimen which fractured at 1.05×10^8 N/m^2. Evidence of both ductile fracture and cleavage is seen, with cleavage apparently following the interface between the Sn matrix and Bi particles which precipitated along crystallographic planes, 3250×.

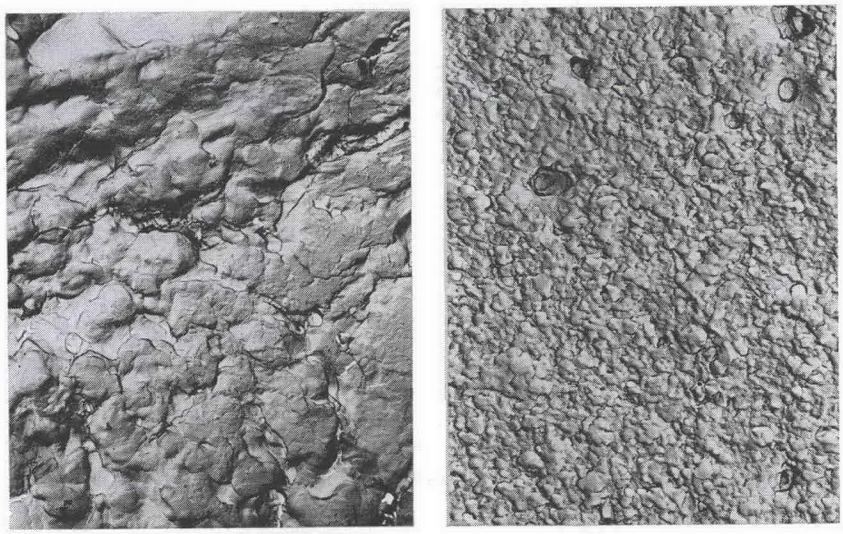

FIG. 11(b), (c). Electron fractographs of 90% Sn–bal Bi specimens which had fractured at (b) 1.55×10^8 N/m^2 and (c) 8.2×10^8 N/m^2 showing a dimpled structure typical of ductile fracture. 3000×.

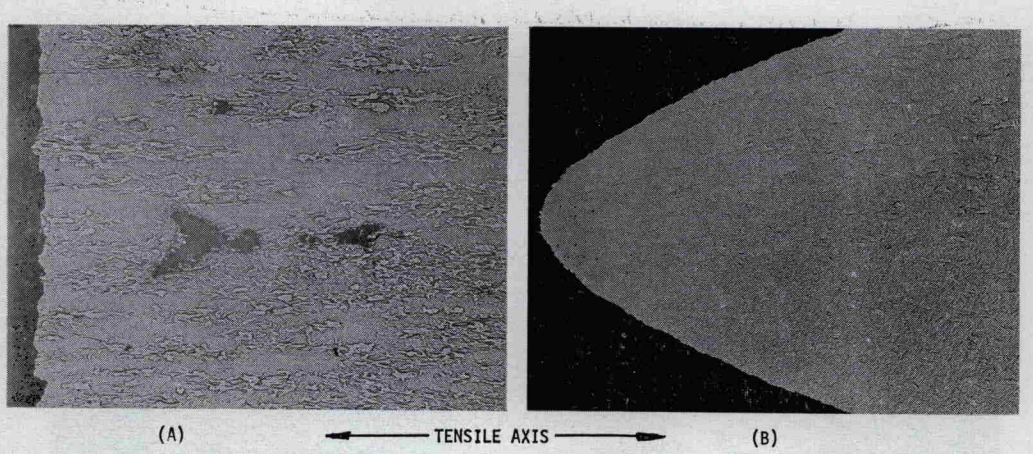

FIG. 12(a), (b). The microstructure of 42% Sn–bal Bi specimens tested to failure at: (a) Atmospheric pressure, showing void formation along the approximate centerline of the specimen. 50×, Etched. (b) 4.3×10^8 N/m², showing ultimate fracture to occur by rupture. 50×, Etched.

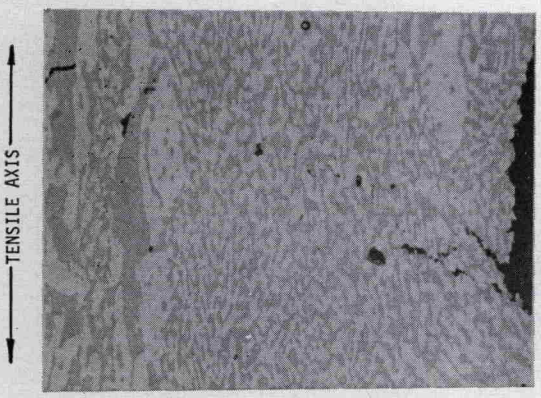

FIG. 12(c). The microstructure of a 42% Sn–bal Bi specimen tested to failure at 1.5×10^7 N/m². Numerous instances of voids occurring at particle-matrix interfaces and evidence of cracking of Bi-rich particles are seen. 500×, Unetched.

and yet the ultimate fracture is along a plane perpendicular to the longitudinal axis. Figure 12(c) shows cracks initiating within Bi particles, and their link-up through the matrix at the edge of the specimen This behavior allows the fracture surface to exhibit macroscopic features typical of brittle fracture even though the alloy is relatively ductile. Figure 12(b) contrasts the appearance of specimens tested to fracture above the BDTP to those fractured at atmospheric pressure (Fig. 12(a)). Here, failure is by rupture with no voids observed along the gauge length.

9 *per cent* Sn–bal Bi *alloys*

Specimens containing a high percentage of primary Bi (i.e. hypereutectic alloys) failed by cleavage within the Bi and ductile failure in the Sn at values of superimposed hydrostatic pressure below the BDTP (Fig. 13) and by rupture at pressures above the BDTP (Fig. 14(a)). Also observed was a change in microstructure in regions of the specimens which had undergone more than minimal deformation prior to fracture. The microstructure shown in Fig. 13 and the post deformation zone area of Fig. 14(b) is representative of the microstructure of this composition, with the Bi grain structure resulting from preferred grain orientation. This "oriented" structure of Bi grains within the primary Bi stringers was destroyed in areas adjacent to the fracture surface (Fig. 14a), and clearly indicated the apparent boundary between deformed and underformed material shown in Fig. 14(b). The final grain structure of these deformed areas was not resolved, an effect felt to be due to recrystallization of these same areas.

FIG. 13. The microstructure of 9% Sn–bal Bi specimens tested to failure at atmospheric pressure, 50×, Unetched, polarized Light.